24-nt phasiRNAs move from tapetal to meiotic cells in maize anthers

Xue Zhou[1], Kun Huang[2,3], Chong Teng[4], Mona Batish[5], Blake C. Meyers[4,6*] and Virginia Walbot[1*]

[1]Department of Biology, Stanford University, Stanford, CA 94305, USA. [2]Department of Plant and Soil Sciences, University of Delaware, Newark, DE 19716, USA. [3]Delaware Biotechnology Institute, University of Delaware, Newark, DE 19716, USA. [4]Donald Danforth Plant Science Center, St. Louis, MO 63132, USA. [5]Department of Medical and Molecular Sciences, University of Delaware, Newark, DE 19716, USA. [6]Division of Plant Sciences, University of Missouri – Columbia, Columbia, MO 65211, USA. *e-mail: bmeyers@danforthcenter.org; walbot@stanford.edu

Abstract

In maize, 24-nt phased, secondary small interfering RNAs (phasiRNAs) are abundant in meiotic stage anthers, but their distribution and functions are not precisely known. Using laser capture microdissection we analyzed tapetal cells, meiocytes, and other somatic cells at several stages of anther development to establish the timing of 24-*PHAS* precursor transcripts and the 24-nt phasiRNA products. By integrating RNA and small RNA (sRNA) profiling plus single-molecule and sRNA FISH (smFISH or sRNA-FISH) spatial detection, we demonstrate that the tapetum is the primary site of 24-*PHAS* precursor and *Dcl5* transcripts and the resulting 24-nt phasiRNAs. Interestingly, 24-nt phasiRNAs accumulate in all cell types, with the highest levels in meiocytes, followed by tapetum. Our data support

24 **the conclusion that 24-nt phasiRNAs are mobile from tapetum to meiocytes and to other**
25 **somatic cells. We discuss possible roles for 24-nt phasiRNAs in anther cell types.**
26
27 In plants, small RNAs (sRNAs) belong to three main categories: microRNAs (miRNAs)
28 involved in target mRNA cleavage, heterochromatic small interfering RNAs (hc-siRNAs)
29 involved in RNA-directed DNA methylation (RdDM), and phased, secondary small interfering
30 RNAs (phasiRNAs). PhasiRNAs were initially reported in male reproductive organs of maize
31 and rice[1-6], and more recently in diverse monocots and eudicots[7-10]; they are found primarily in
32 anthers. In most species, 21-nt phasiRNAs predominate during early anther development, while
33 24-nt phasiRNAs are abundant during meiosis.
34 PhasiRNA biogenesis starts with transcription of long noncoding precursors (*PHAS*
35 transcripts) by RNA polymerase II. Subsequently, the *PHAS* transcripts are capped and
36 polyadenylated, translocated to the cytoplasm, and then bound by ribosomes[11]. In the polysomal
37 complex, an Argonaute-associated 22-nt miRNA complementary to sequences in the *PHAS*
38 transcript binds to this precursor molecule and triggers cleavage. miR2118 is utilized for most
39 21-nt *PHAS* precursors and miR2275 for most 24-nt *PHAS* precursors based on the presence of
40 complementary sequences; a fraction of precursors lacks such complementarity and may be
41 processed utilizing other miRNAs. Then, the 3′ portions of cleaved transcripts are converted to
42 double-stranded RNA by RNA-DEPENDENT RNA POLYMERASE 6 (RDR6), and
43 subsequently processed by Dicer-like proteins (DCL4 for the 21-nt and DCL5 for the 24-nt type)
44 to yield the phasiRNAs[1,2,4,12]. Despite the expectation of equal stoichiometry of all the products
45 from one *PHAS* transcript, individual phasiRNA abundances derived from the same transcript

46 can differ by more than 1000-fold indicating differential stabilization[6,13]. It is possible that only
47 these few abundant products generated from one precursor have functions.
48 In maize the 21-nt phasiRNAs are distributed throughout immature anther lobes based on
49 *in situ* hybridization with one or a few examples, although the production of miR2118 is
50 restricted to the epidermis[1]. Several observations associate phasiRNAs with male sterility. First,
51 the absence of specific 21-nt phasiRNAs are implicated in causing male sterility in rice[14,15].
52 Second, in numerous male-sterile mutants of maize, either the 21-nt or 24-nt phasiRNAs are
53 absent reflecting the tight control of the normal timing of their appearance during
54 development[1,2,16,17]. More specifically addressing the role of 24-nt phasiRNAs, *dicer-like5*
55 mutants unable to process most 24-nt *PHAS* precursors are male-sterile and exhibit aberrant
56 tapetal development under normal growing conditions[2]. In maize, the expression of *PHAS*
57 precursors and miR2275 as well as the accumulation of 24-nt phasiRNAs occur mainly in the
58 tapetum at the prophase I stage in anthers[1]. Male-sterile mutants with tapetal developmental
59 defects evident during early meiotic stages are missing the 24-nt phasiRNAs[2,17]. Interestingly,
60 the male sterility cases in rice and maize exhibit temperature-dependent male sterility: in
61 appropriate growing conditions, the plants are male-fertile despite the absence of specific or an
62 entire class of phasiRNAs[2,15,16]. This observation has led to the hypothesis that phasiRNAs may
63 buffer anther development against environmental perturbation, particularly in the tapetum. In
64 addition to the expectation that phasiRNAs could modulate mRNA half-life of still poorly
65 defined targets, the 24-nt phasiRNAs result in increased CHH DNA methylation at 24-*PHAS* loci
66 in maize, as assessed in whole anthers[13]. In analysis of isolated meiocytes, 24-nt phasiRNAs
67 have been detected, and there is an increase in CHH DNA methylation, leading to the hypothesis
68 that these phasiRNAs might regulate meiosis[18] by an unknown mechanism related to *cis*

69 methylation of their own loci. To date, the precise role of 24-nt phasiRNAs in regulating maize
70 anther development has remained elusive.

71 sRNAs can function by travelling within and between organs: from the site of synthesis,
72 they can spread both to neighboring cells and systemically over long distance[19-21]. Cell-to-cell
73 movement of sRNAs is probably through plasmodesmata (PD), a plasma membrane-lined pore
74 acting as an intercellular channel that connects the cytoplasm of adjacent cells[22]. To date, the
75 potential movement of 24-nt phasiRNAs from the site of biogenesis to the neighboring cell
76 layers in maize anthers has not been well studied. A major concern with our previous localization
77 analysis for 24-nt phasiRNAs and biogenesis components primarily to the tapetum is that only a
78 few examples were evaluated, and the probes can adhere to the callose coat surrounding the
79 germinal cells, yielding a non-specific signal[1]. Therefore, in meiotic stage maize anthers, two
80 major questions should be addressed: 1) do meiocytes contain all the components for generating
81 24-nt phasiRNAs? And, 2) using RNA-seq and small RNA-seq, what is the timing of synthesis
82 and the distribution of these components in anther lobes?

83 To explore the distribution of 24-nt phasiRNA biogenesis components and the resulting
84 small RNAs, we used laser capture microdissection (LCM) to isolate meiocytes (ME), tapetum
85 (TAP), and other somatic cells (OSC) from two anther developmental stages for low input RNA-
86 seq and sRNA-seq and for a more comprehensive developmental analysis using RT-qPCR. By
87 integrating comprehensive RNA/sRNA profiling and single-molecule or sRNA FISH
88 (smFISH/sRNA-FISH) spatial detection, we demonstrate that TAP contain the most 24-*PHAS*
89 primary transcripts, whereas ME ultimately accumulate more 24-nt phasiRNAs at meiotic
90 prophase I. We discuss these results in a model in which 24-nt phasiRNAs move from TAP to
91 ME during meiosis.

92 **Results**

93 **LCM collections from meiotic stage maize anthers**

94 Control of fertility in maize anthers, the male reproductive floral organs, is important for hybrid
95 seed production as an economic way to improve grain yield. Maize tassels produce hundreds of
96 spikelets, each of which contains an upper and lower floret, and each floret contains three anthers
97 (Fig. 1a). The lower floret stamens develop approximately 1 day later than the upper floret
98 stamens within the same spikelet. At the beginning of meiosis, each anther contains four lobes;
99 each lobe consists of four somatic cell types that are required to support the meiotic cell
100 development (Fig. 1a). The high regularity of maize anther development, numerous anthers, and
101 a detailed staging system allow rapid dissection of carefully staged anthers for cytological and
102 molecular analysis[23] (Fig. 1b, c). To explore the spatial distribution of 24-nt phasiRNAs and their
103 pathway components in the W23 inbred (Fig. 2a), LCM was used to isolate three samples (ME,
104 TAP, and OSC) from two stages of meiotic anthers (1.5 mm zygotene and 2.0 mm pachytene)
105 (Supplementary Fig. 1 and Supplementary Table 1). Collections from additional stages were
106 used in RT-qPCR analysis to provide finer detail of the timing of biogenesis of a subset of 24-
107 *PHAS* precursor and *Dcl5* transcripts.

108

109 **24-*PHAS* precursors accumulate in tapetal cells**

110 Seventeen RNA-seq libraries were built from ME, TAP, and OSC recovered from 1.5 mm and
111 2.0 mm stage anthers plus single, fixed anthers (FA) (Supplementary Table 2). To check the
112 reproducibility of the datasets, a correlation heatmap and a Principal Component Analysis (PCA)
113 plot were constructed (Fig. 1d, e). Biological replicates are highly similar and distinct from other
114 cell collections at both stages, confirming the high quality of our LCM sample collections. 126

115 (TPM > 0) of 176 previously discovered 24-*PHAS* precursor types were identified in FA and
116 LCM cell sample collections[1] (Supplementary Table 3); *PHAS* precursors that overlapped
117 protein coding genes were excluded. As shown in Fig. 2b, 118 of these loci had sufficient and
118 reliable expression (TPM reads > 5 in at least one sample) for further analysis. Overall, the 24-
119 *PHAS* precursors were most abundant in TAP at the 1.5 mm stage, showing an expression
120 pattern and high abundance similar to that in 1.5 mm FA (Fig. 2b); therefore, the majority of 24-
121 *PHAS* precursors in whole anthers are found in the tapetal cells. The average total expression
122 levels of 24-*PHAS* loci are approximately 65 times lower in ME and 20 times lower in OSC at
123 this zygotene stage (Fig. 2b and Supplementary Table 3). Single cell RNA-seq (scRNA-seq)
124 analysis of individual ME detected a low abundance of 24-*PHAS* loci during the pre-
125 zygotene/zygotene stages in a A188/B73 maize hybrid stock[24]. The total average abundance of
126 these 24-*PHAS* transcripts per zygotene sample in A188/B73 is less than that in the pooled
127 meiocyte LCM samples at 1.5 mm from W23 maize anthers. Furthermore, our previous scRNA-
128 seq data also identified extremely low abundances of 24-*PHAS* precursors in premeiotic AR and
129 PMC in W23 maize anthers[25]. These data suggests that the TAP is the main source for 24-*PHAS*
130 precursors in zygotene stage maize anthers.

131 To further verify our LCM RNA-seq data and to quantify transcripts in more stages, we
132 randomly selected three highly expressed 24-*PHAS* precursors (*PHAS15*, *PHAS116*, and
133 *PHAS296*) for smFISH and RT-qPCR assays (Fig. 2c). In the LCM RNA-seq data, transcripts for
134 all three loci were significantly enriched in TAP at the 1.5 mm stage compared to ME and OSC
135 (Supplementary Fig. 2). smFISH images confirmed that TAP contain most of these three 24-
136 *PHAS* transcripts (yellow dots resulting from dye AF647 labeling) at the 1.25 mm and 1.5 mm
137 stages during late leptotene/pre-zygotene and zygotene stages in W23 anthers (Fig. 2d, g and

138 Supplementary Fig. 3a). Quantification counts (transcript count) demonstrated that TAP is
139 significantly higher at both stages (Fig. 2e, h and Supplementary Fig. 3b). Almost no expression
140 was detected at earlier or later stages (Fig. 2d, e, g, h and Supplementary Fig. 3a, b) or in control
141 hybridization assays (Supplementary Fig. 4). For RT-qPCR using W23 anthers and LCM
142 samples, *ZmCyanase* was used as the internal reference; it is consistently expressed across all
143 anther stages and is expressed in all cell layers based on smFISH detection (Supplementary Fig.
144 5) compared to the no label control hybridization test (Supplementary Fig. 6). In 0.75-2.5 mm
145 W23 maize anthers, the expression patterns of the three 24-*PHAS* loci showed a similar pattern,
146 with high expression levels in both 1.25 mm and 1.5 mm anthers and with significant enrichment
147 in TAP compared to ME and OSC (Fig. 2f, i and Supplementary Fig. 3c).

148 To further solidify the conclusion that TAP is the primary site of 24-*PHAS* transcript
149 biogenesis, we utilized the *dcl5-mu3* mutant. Several *dcl5* mutants have been documented to
150 contain normal 24-*PHAS* precursor levels but lack virtually all the 24-nt phasiRNAs[2]. We
151 reasoned that in the absence of the processing machinery, the large 24-*PHAS* precursors would
152 accumulate in the cells where they were synthesized. This was indeed true as the *PHAS116*
153 transcripts were found to be highly enriched in TAP at the 1.75 mm stage (this is a slightly later
154 stage than in W23 anthers) in homozygous *dcl5* (*dcl5-mu03//dcl5-mu03*) anthers (mixed inbred
155 background) using smFISH (Fig. 2j).

156 Overall, these data demonstrate that maize tapetal cells are the main site for 24-*PHAS*
157 precursor accumulation and that accumulation starts at early meiotic prophase I and peaks during
158 zygotene. We also established that accumulation is already substantial at the initial stages of
159 meiosis in 1.25 mm anthers, approximately one day earlier than detected previously by analysis
160 of 1.0 mm and 1.5 mm W23 whole anthers[1].

161 **The spatial distribution of 24-nt phasiRNA biogenesis pathway components**

162 Argonaute (AGO) proteins, binding partners of miRNAs and phasiRNAs, play essential roles in
163 phasiRNAs biogenesis and RNA silencing (RNAi)[26,27]. AGOs are assumed to be involved at two
164 steps in 24-nt phasiRNA biogenesis and function: a specific AGO as the binding protein for the
165 miR2275 trigger and one or several AGOs as the binding proteins for the diverse 24-nt
166 phasiRNAs (Fig. 2a). We identified transcripts encoding 18 AGO proteins in LCM cell
167 collections (Fig. 3a). Nine AGO protein transcripts were expressed in one or two cell collections,
168 and the other nine AGO proteins were detected in all three cell collections. None of the AGO
169 isotype transcripts were specific to tapetal cells. Fifteen of 18 AGO members were expressed in
170 TAP at the 1.5 mm stage, providing a list of AGOs that could be involved in 24-nt phasiRNA
171 biogenesis (Fig. 3a). Among these, AGO1 family members have already been designated as
172 candidates in previous studies in maize and rice[5,7, 28], and now three AGO members (AGO10b,
173 AGO2b, and AGO5c) not expressed in 1.5 mm TAP can likely be excluded as candidates for 24-
174 nt phasiRNA biogenesis (Fig. 3a). In meiocytes, transcripts were found for 11 AGO proteins,
175 many of which were more highly expressed in ME than other cell types, but none were exclusive
176 to ME (Fig. 3a). Several of these AGO types were predicted in previous transcriptome profiling
177 and spatial localization studies to be potential 24-nt phasiRNA binding partners, such as AGO18
178 family members[1, 5, 29] and AGO2b[5] based on the timing of their expression. It is noteworthy that
179 we detected abundant *AGO5c* transcripts, and these were enriched in ME and absent in TAP
180 (Fig. 3a). AGO5c is encoded by the maize *male-sterile28* gene and is homologous to rice
181 MEL1[30], which is the binding partner for a subset of 21-nt phasiRNAs in rice[14].

182 We investigated the transcript abundance of *Dcl5* and *Rdr6* in the LCM RNA-seq data.
183 *Dcl5* was significantly higher in TAP at the 1.5 mm stage than any other samples (Fig. 3b). In

184 contrast, *Rdr6* was expressed in all three cell collections, with slightly higher expression levels in
185 ME, followed by TAP at both stages (Fig. 3b). To precisely pinpoint the timing of expression,
186 RT-qPCR demonstrated that *Dcl5* transcripts were significantly higher in TAP samples (Fig. 3c);
187 furthermore, the expression pattern of *Dcl5* is similar to the three 24-*PHAS* precursors (*PHAS15*,
188 *PHAS116*, and *PHAS296*), with the highest expression levels detected in TAP compared to ME
189 or OSC at both 1.25 mm and 1.5 mm stages (Fig. 3c). As shown in Fig. 3d-f with smFISH
190 detection, *Dcl5* transcripts (yellow dots resulting from dye Texas Red labeled smFISH probes)
191 were prominently localized in TAP at the 1.25 mm, 1.5 mm, and 1.75 mm stages in either W23
192 anthers or heterozygous *Dcl5*//*dcl5* fertile anthers. Far fewer yellow dots were detected in ME or
193 OSC, and almost no signal was detected in the negative control samples (Fig. 3f and
194 Supplementary Fig. 6). An additional smFISH analysis of *Dcl5* using AF647 labeled smFISH
195 probes confirmed that *Dcl5* transcripts were localized mainly in TAP at 1.25 mm and 1.5 mm
196 (Supplementary Fig. 7). These data suggest that TAP is the main site for *Dcl5* accumulation at
197 early meiotic prophase I in maize.

198 Previous studies have reported that four basic helix-loop-helix (bHLH) factors (*Ms23*,
199 *Ms32*, *bHLH52*, and *bHLH122*) are required for normal tapetal cell specification and
200 differentiation in maize[17,31]. *Ms23* is the master transcription factor (TF) and is required for
201 expression of 24-*PHAS* precursors, miR2275, and 24-nt phasiRNAs[1]. Here, *Ms23* and *bHLH51*
202 were highly expressed in TAP at 2.0 mm, whereas *Ms32* and *bHLH122* were more abundant in
203 TAP at 1.5 mm (Supplementary Fig. 8). These TF expression patterns are consistent with our
204 previous work in maize anthers, particularly the absence of *bHLH122* transcripts at 2.0 mm[17].
205 Importantly, the TAP is significantly higher for these four TFs compared with the other two cell
206 collections (Supplementary Fig. 8). Collectively, the distribution of key TFs by RNA-seq and

207 localization data provide further evidence that TAP is the main site for transcription of *PHAS*
208 precursors and their processing into 24-nt phasiRNAs. Based on the timing of 24-*PHAS*
209 accumulation, heterodimers of *Ms32* and *bHLH122* are candidates for direct regulation of 24-
210 *PHAS* loci. Because *Ms23* is essential for expression of *bHLH122,* it is also a critical factor.
211

212 **24-nt phasiRNAs are abundant in all three cell collections**

213 To investigate the spatial distribution of 24-nt phasiRNAs in meiotic stage anthers, we collected
214 ME, TAP, and OSC by LCM from 1.5 mm and 2.0 mm W23 maize anthers for low input sRNA-
215 seq (Supplementary Table 1, 2). We first classified sRNAs by length (18 nt to 30 nt) in FA and
216 LCM cell collections. Confirming previous results[1], the 24-nt size sRNA class is the most
217 abundant at both stages (Supplementary Fig. 9a). The 21-nt size sRNA class is also detectable,
218 but with lower expression levels (Supplementary Fig. 9a). Using the set of 118 24-*PHAS* loci for
219 analysis (Fig. 2b), 24-nt phasiRNAs from these loci were more abundant in all three cell
220 collections at 2.0 mm than at the 1.5 mm stage (Fig. 4a and Supplementary Table 3). The
221 expression patterns of 24-nt phasiRNAs and 22-nt miR2275 family members are very similar,
222 with the highest abundance in ME at 2.0 mm during pachytene, followed by TAP at this stage
223 (Fig. 4a). A previous sRNA-FISH co-localization study reported that miR2275 and one 24-nt
224 phasiRNA had higher abundances in AR/ME and TAP in maize anthers[32]. Here, two of the
225 miR2275 family members (miR2275a and miR2275b) were highly expressed, indicating they
226 might play key roles in 24-*PHAS* precursor cleavage (Fig. 4b). Although the precursors are most
227 abundant in TAP cells (Fig. 2b, c and Supplementary Fig. 2), the 24-nt phasiRNAs accumulate to
228 higher levels in the ME (Fig. 4a, c and Supplementary Fig. 9b). Individual 24-nt sRNA
229 abundances from products of the same locus (*PHAS15*, *PHAS116*, and *PHAS296*) are not

230 uniform: only a few of the 24-nt sRNAs show high abundance despite the expectation of equal
231 stoichiometry from a single precursor molecule (Fig. 4d, e and Supplementary Fig. 10a).
232 Furthermore, sRNAs localization studies illustrated that 24-nt phasiRNAs from three 24-*PHAS*
233 loci (*PHAS15*, *PHAS116*, and *PHAS296*) were expressed in all three cell types, with higher
234 expression levels in ME and TAP, lower in OSC from 1.25 mm to 2.0 mm (Fig. 4f, g and
235 Supplementary Fig. 10b). Almost zero expression, considered to be background, was detected in
236 control hybridization assays (no labeled control and mouse HKH RNA control) (Fig. 4f, g and
237 Supplementary Fig. 10c). These distribution patterns lead us to hypothesize that the TAP is the
238 site for nearly all 24-nt phasiRNAs biogenesis and that the presence of 24-nt phasiRNAs in ME
239 and OSC depends on transport during early meiotic prophase I in maize.
240

241 **Discussion**

242 In anthers, TAP is the innermost of the four somatic layers, adjacent to the germinal cells. The
243 TAP plays essential roles in providing nutrients, enzymes, and pollen wall components to
244 support AR, ME, and microspore (MSP) development. Defects in tapetal function or the
245 abnormal differentiation of TAP usually leads to meiotic arrest or to later pollen abortion[2,17,31,33-
246 35]. 24-nt phasiRNAs have been reported as abundant in meiotic stage maize anthers from
247 hundreds of unique copy loci[1]. In TAP-defective, male-sterile mutants lacking key tapetal-
248 expressed TFs, almost all the 24-nt phasiRNAs are missing[1,17], which indicates that TAP is likely
249 to be involved in 24-nt phasiRNA biogenesis. Our low-input RNA-seq data for ME, TAP, and
250 OSC demonstrated that the TAP is the main source for the 118 24-*PHAS* precursor transcripts as
251 well as *Dcl5* transcripts in 1.5 mm stage anthers (Fig. 2b, c and Fig. 3b), confirming a previous
252 study in the same W23 background that 1.5 mm anthers were the peak stage for 24-*PHAS* loci

253 production with 1.0 mm anthers lacking expression[1]. We further refined the timing using
254 smFISH and RT-qPCR assays, demonstrating that three selected 24-*PHAS* loci (*PHAS15*,
255 *PHAS116*, and *PHAS296*) and *Dcl5* transcripts were initially expressed at 1.25 mm during the
256 leptotene-zygotene transition and were continuously expressed at 1.5 mm or 1.75 mm during
257 zygotene (Fig. 2d-i, 3d-f and Supplementary Fig. 3, 7). Moreover, the earlier timing for 24-nt
258 phasiRNA generation corresponds to the stage just prior to and including the leptotene-zygotene
259 transition (Fig. 4f, g and Supplementary Fig. 10b), which is a key checkpoint in meiosis. A
260 previous study has reported that CHH DNA methylation is elevated in isolated ME, specifically
261 at the phasiRNA-producing loci[18]. Therefore, a logical hypothesis is that some of the 24-nt
262 phasiRNAs generated in the TAP and transported to ME might induce methylation in the
263 corresponding loci. It is unclear how such *cis* methylation could contribute to meiotic regulation.
264 Furthermore, in *dcl5* mutants, meiosis is normal in the near complete absence of 24-nt
265 phasiRNAs[2], indicating that whatever role the 24-nt phasiRNAs play, it is dispensable.
266 By using LCM-purified cell collections, our data demonstrate that TAP cells are the
267 primary site of 24-*PHAS* precursor accumulation and 24-nt phasiRNA biogenesis. sRNA-seq
268 data for ME, TAP, and OSC illustrated that 24-nt phasiRNAs and miR2275 family members
269 were found in all three cell collections, with higher expression levels in ME at 2.0 mm during
270 pachytene, followed by TAP at the same stage (Fig. 4a-c). Furthermore, sRNA-FISH detection
271 confirmed that the 24-nt phasiRNAs originating from three 24-*PHAS* loci (*PHAS15*, *PHAS116*,
272 and *PHAS296*) were present in all three cell layers from 1.25 mm to 2.0 mm (Fig. 4f, g and
273 Supplementary Fig. 10b). Our major new conclusion is the proposal that 24-nt phasiRNAs
274 generated in the TAP move to other cell types. This conclusion is summarized in a model of 24-
275 phasiRNA biogenesis and mobility in maize anthers during meiotic prophase I (Fig. 5). We

276 demonstrated that TAP is the main site of 24-nt phasiRNAs biogenesis, as TAP contain the most
277 of 24-*PHAS* precursors, *Dcl5* transcripts, adequate miR2275, and *Rdr6*. To understand why ME
278 later contain the highest levels of 24-nt phasiRNAs, we note that there are approximately 30
279 tapetal cells touching each ME, whereas only approximately 0.6 tapetal cell touch neighboring
280 OSC[23]. Utilizing the LCM cell numbers we recovered and the total 24-nt phasiRNA reads we
281 generated (Supplementary Table 1, 3b), we calculated that each tapetal cell "donates"
282 approximately 5% of its 24-nt phasiRNAs to ME or OSC during meiotic prophase I in maize
283 anthers. If each TAP cells exports 5% (5 units) of its 24-nt phasiRNAs to ME cells, each ME
284 would have 5 units x 30 = 150 units of 24-nt phasiRNAs, therefore reaching a higher level than
285 the source TAP cells. In contrast, export of 5 units of 24-nt phasiRNAs to the OSC, would result
286 in a low level of 24-nt phasiRNAs in the immediate receiving middle layer cell with further
287 dilution as 24-nt phasiRNAs move throughout the OSC group. A challenge for future research
288 will be documenting the path of 24-nt phasiRNA movement. Other cases of plant intercellular
289 movement of sRNAs are probably through PD, regulating tissue or organ development by genes
290 silencing and RdDM[22]. PD are membrane-lined intercellular channels that connect the
291 cytoplasms of adjacent cells, such as between TAP and PMC/ME or non-TAP somatic cells in
292 anthers[36,37]. Therefore, we speculate that 24-nt phasiRNAs move from the biogenesis site in TAP
293 to ME or OSC through PD in meiotic prophase I maize anthers.

294 In *Arabidopsis*, tapetal-derived 24-nt siRNAs induce DNA methylation in the germline
295 and maintain genome integrity by silencing corresponding genes and transposons[38]. Here, 24-nt
296 phasiRNAs are generated in TAP and then exported to ME (Fig. 5). These exported 24-nt
297 phasiRNAs are likely required for the elevated CHH DNA methylation at 24-*PHAS* loci in
298 isolated ME in maize[18]. In *Arabidopsis*, the 24-nt siRNAs appear to have a broader role in

299 modifying the ME genome and gene expression than the 24-nt phasiRNAs have in maize. This is
300 particularly true for any impact 24-nt phasiRNAs might have on gene expression, because no
301 mRNA targets for this class of small RNAs have been identified. Nonetheless, it is interesting
302 that small RNAs synthesized in the TAP are transferred to maize ME. Analysis of *dcl5* maize
303 mutants establishes that in the absence of 24-nt phasiRNA biogenesis, tapetal cells fail to
304 differentiate properly at normal maize growing temperatures (28 °C), while meiosis proceeds
305 normally[2]. These observations indicate that the 24-nt phasiRNAs play an essential role in the
306 TAP -- not in ME -- during the meiotic stages; later, microspore failure renders *dcl5* mutants
307 male-sterile, a fact that we attribute to the failure of the tapetum to supply nutrients and wall
308 components to the developing uninucleate microspores. Mutants grown at low temperature
309 (21 °C) are fertile and tapetal development is slow but sufficient indicating that 24-nt phasiRNAs
310 are not required under these conditions. Considering these observations *in toto,* it is possible that
311 in maize the transfer of 24-nt phasiRNAs to meiocytes is an evolutionary relic that no longer
312 serves (or fully serves) a required function and that the primary role of the 24-nt phasiRNAs is to
313 support rapid tapetal differentiation.

314 **Methods**

315 **Plant materials**

316 Maize (*Zea mays*) W23 *bz2* inbred line plants were grown in Stanford, CA, USA under
317 greenhouse conditions (31 °C/21 °C, 14 h day/10 h night light cycle with supplemental LED and
318 UV-A lamps providing ~50% of summer sun conditions). Anthers were dissected from tassels
319 and then measured using a micrometer (Fisher Scientific).

320 Homozygous *dcl5-mu03//dcl5-mu03* plants are temperature-sensitive male sterile. They
321 are male sterile under optimized growth condition (28 °C/22 °C day/night temperature, 14 h
322 light, 400 μmol/m^2/s) in the greenhouse. *dcl5-mu03//dcl5-mu03* male sterile and *dcl5-*
323 *mu03//Dcl5* fertile siblings were grown in St. Louis, MO, USA under the optimized growth
324 conditions in a greenhouse.

325

326 **Laser Capture Microdissection (LCM)**

327 ME, TAP, and OSC were isolated from 1.25 mm, 1.5 mm, and 2.0 mm W23 anthers by LCM as
328 described previously[39], with minor modification. Fixed anthers were cryoprotected in 10% (2-3
329 days) and 15% sucrose/PBS (phosphate buffered saline) (5 to 7 days) to better preserve tapetal
330 cell layer morphology. Total RNA was isolated from each cell type using the RNAqueous™-
331 Micro Kit (Invitrogen); RNA quality was evaluated on an Agilent Bioanalyzer using the RNA
332 6000 Pico Kit (Agilent Technologies).

333

334 **Cytological staging and imaging**

335 AR/PMC/ME from W23 anthers (from the 0.75 mm through 2.25 mm anther length stages,
336 recovered at 0.25 mm intervals) were extruded, classified using a micrometer, and then

337 appropriately sized anthers were stained with 10 μg/mL Hoechst 33342 (Sigma-Aldrich)
338 according to our pervious report[25]. Confocal image stacks for the germinal cells were taken with
339 a Leica SP8 microscope using a 93X Glycerol immersion objective. ImageJ[40] was used for
340 processing the fluorescent microscopy images. Cytological stages during meiotic prophase I
341 were assigned using established criteria[25,41].
342
343 **RNA-seq and sRNA-seq library construction and sequencing**
344 Total RNA was isolated from three different LCM cell samples and FA samples at 1.5 mm and
345 2.0 mm using the RNAqueous™-Micro Kit (Invitrogen). RNA-seq libraries were prepared using
346 CEL-seq2[42] based on a modified protocol[25]. Primers were synthesized by phosphoramidite
347 chemistry at the Stanford Protein and Nucleic Acid Facility (Stanford, CA) (Supplementary
348 Table 4). All RNA-seq libraries were sequenced on an Illumina HiSeq 4000 instrument at the
349 Stanford Genome Sequencing Service Center (Stanford, CA) with paired-end 150 bp reads.
350 For small RNA library preparation, RealSeq®-AC kits (SomaGenics) were used for ultra-
351 low amounts of total RNA starting with 100 ng from whole anthers or 10 ng from LCM cell
352 samples. Sequencing in a single-end mode on an Illumina NextSeq (University of Delaware)
353 yielded 75 bp reads for sRNA-seq.
354
355 **Data handling and bioinformatics**
356 Paired-end RNA-seq Read1 contained a 10 bp unique molecular identifier (UMI)[43] and sample
357 barcodes, and Read2 contained the transcript sequence. Each UMI was processed and attached to
358 the Read2 metadata using fastp[44]. Barcodes were used to demultiplexed Read2 into a separate
359 file for each library using fastq-multx[45]. After trimming the adapters by Trim Galore, the reads

360 were mapped to version 4 of the B73 maize genome using Hisat2[46]. RNA-seq reads were
361 normalized by dividing by the total number of transcripts (UMIs) in each sample and multiplying
362 by one million (transcripts per million normalization).
363 sRNA-seq data were processed as previously described[47]. In brief, Trimmomatic version
364 0.32[48] was used to remove the linker adaptor sequences. Then, the trimmed reads were mapped
365 to version 4 of the B73 maize genome using Bowtie[49]. Read counts were normalized to one
366 million to allow for the direct comparison across libraries. PhasiRNAs were designated based on
367 the criteria of a 24-nt length and mapping coordinates within the previously identified 176 *24-*
368 *PHAS* loci[1] that were updated to version 4 of the B73 genome using the assembly converter
369 tool[50].
370
371 **Quantitative reverse transcription PCR (RT-qPCR)**
372 RT-qPCR for multiple stage anthers (0.75 mm – 2.0 mm; 0.25 mm intervals) and LCM cell
373 sample collections (ME, TAP, and OSC) was performed using the Luna® Universal Probe One-
374 Step RT-qPCR Kit (New England Biolabs). Quantitative PCR was performed using TaqMan
375 primers synthesized by Integrated DNA Technologies (Table S5) on a CFX96 C1000 Touch
376 Real-Time PCR Detection System (BioRad). *ZmCyanase* expression was used to normalize
377 among biological samples, because this gene is highly expressed at all stages of anther
378 development (Supplementary Fig. 5). Each sample type was tested in two biological and three
379 technical replicates.
380
381 **Single-molecule fluorescence *in situ* hybridization (smFISH) for mRNAs and sRNAs**

382 Maize spikelets of various sizes were dissected from the central spike and fixed in 20 mL glass
383 vials using 4% paraformaldehyde in 1x PHEM buffer (5 mM HEPES, 60 mM PIPES, 10 mM
384 EGTA, 2 mM $MgCl_2$ pH 7). Fixation was done three times in a vacuum chamber at 0.08 MPa, 15
385 min each. After fixation, samples were sent for paraffin embedding at the histology lab in the
386 Nemours/Alfred I. duPont Hospital for Children (Wilmington, DE). Embedded paraffin samples
387 were sectioned using a paraffin microtome and dried on poly-l-lysine-coated 22 x 22 mm #1.5
388 coverslips (Carl Zeiss Microscopy, LLC, Cat# 474030-9020-000). Samples were then de-
389 paraffinized using Histo-Clear (Fisher Scientific, 50-899-90147) and re-hydrated by going
390 through an ethanol series of 100, 95, 80, 70, 50, 30, 10% (vol/vol) (30 sec each) and finally water
391 (1 min) at room temperature. After protease (Sigma, P5147) digestion (20 min, 37°C), samples
392 were neutralized in 0.2% glycine (Sigma-Aldrich, G8898) for 2 min. After two washes in 1x
393 PBS buffer, samples were dehydrated and then hybridized with smFISH probes. About 20-nt
394 smFISH probes were designed to bind specifically across the length of each target RNA in a non-
395 overlapping series[51]. For small RNA detection, probes were designed reverse complemented to
396 ~19 nt of the phasiRNA sequences generated from each locus. Briefly, 23-51 probes (total
397 coverage of about 800 nt for mRNAs or sRNAs) were designed for each target, and each probe
398 was synthesized with a 3' amino modification (LGC Biosearch Technologies, CA)
399 (Supplementary Table 6). All the probes of one set were pooled and *en masse* coupled with
400 Alexa Fluor 647 (Thermo Fisher) or Texas Red; the labeled probe fraction was purified using
401 reverse phase HPLC[52]. The probes were diluted to a concentration of 20 ng/ul in a hybridization
402 buffer containing 10% formamide, 1 mg/mL yeast tRNA, 10% dextran sulfate and 2 mM
403 Vanadyl ribonucleoside complex (New England Biolab, Ipswich, MA, Catalogue Number,
404 S142), 0.02% RNase free BSA (Ambion, AM2618). The biological samples were hybridized

405 with hybridization mix overnight in a humid chamber at 37°C. The samples were then washed
406 two times with 2X SSC buffer (sodium saline citrate) containing 10% formamide, and a final
407 wash was done using 1X TBS buffer (Tris-buffered saline). Samples were mounted using
408 ProLong™ Glass Antifade Mountant with NucBlue™ Stain (ThermoFisher Scientific, P36981).
409 Fluorescence was detected by spectral unmixing of autofluorescence spectra using laser
410 scanning confocal microscopy on a Zeiss LSM 880 multiphoton confocal microscope. We used
411 30% power of the 633 nm laser and an alpha Plan-Apochromat 100x/1.46 oil lens to acquire
412 RNA *in situ* images. Pure dye was used as positive control, and autofluorescence from maize
413 tissue was used as the negative control for spectral bleed-through. After images were acquired,
414 each image was spectra unmixed. The brightness and contrast of images in the same figure panel
415 were adjusted equally and linearly in Zen 2010 (Carl Zeiss). For quantification, the numbers for
416 each localization event were calculated using ImageJ (SpotQuant). Two replicates for each Z-
417 stack of images were used for calculating the copy number for each gene's transcripts.
418

419 **Acknowledgements**

420 We thank M. Zhang for initial suggestions on project design and for instructing X. Zhou in the
421 LCM technique; B. Nelms for help with low input RNA-seq library construction and raw data
422 processing; Y. Chan and Y. Liu for help in data handling; J. Caplan for helpful advice on
423 smFISH; J. Zhan assisted retrieval and organization of the sequences of 24-*PHAS* precursors and
424 24-nt phasiRNAs; and J. Dinneny for use of the SP8 confocal microscope. This project was
425 supported by National Science Foundation award 17540974.
426

427 **Author contributions**

X.Z., B.C.M, and V.W. conceived and designed the project. X.Z. performed most of the experiments and bioinformatics. K.H. and M.B. designed and synthesized smFISH probes. K.H. performed smFISH and imaging analysis. T.C. constructed sRNA libraries and performed raw data processing. X.Z. and V.W wrote the manuscript with editing by B.C.M. and K.H. and with contributions from all co-authors.

Competing interests

The authors declare no competing interests.

436 **Reference**

437

438 1 Zhai, J. *et al.* Spatiotemporally dynamic, cell-type-dependent premeiotic and meiotic
439 phasiRNAs in maize anthers. *Proc Natl Acad Sci U S A* **112**, 3146-3151,
440 doi:10.1073/pnas.1418918112 (2015).
441 2 Teng, C. *et al. Dicer-like5* deficiency confers temperature-sensitive male sterility in
442 maize. *Nat Commun* **11**, 2912, doi:10.1038/s41467-020-16634-6 (2020).
443 3 Johnson, C. *et al.* Clusters and superclusters of phased small RNAs in the developing
444 inflorescence of rice. *Genome Res* **19**, 1429-1440, doi:10.1101/gr.089854.108 (2009).
445 4 Song, X. *et al.* Roles of DCL4 and DCL3b in rice phased small RNA biogenesis. *Plant J*
446 **69**, 462-474, doi:10.1111/j.1365-313X.2011.04805.x (2012).
447 5 Fei, Q. *et al.* Dynamic changes of small RNAs in rice spikelet development reveal
448 specialized reproductive phasiRNA pathways. *J Exp Bot* **67**, 6037-6049,
449 doi:10.1093/jxb/erw361 (2016).
450 6 Tamim, S. *et al.* Cis-directed cleavage and nonstoichiometric abundances of 21-
451 nucleotide reproductive phased small interfering RNAs in grasses. *New Phytol* **220**, 865-
452 877, doi:10.1111/nph.15181 (2018).
453 7 Kakrana, A. *et al.* Plant 24-nt reproductive phasiRNAs from intramolecular duplex
454 mRNAs in diverse monocots. *Genome Res* **28**, 1333-1344, doi:10.1101/gr.228163.117
455 (2018).
456 8 Xia, R. *et al.* 24-nt reproductive phasiRNAs are broadly present in angiosperms. *Nat*
457 *Commun* **10**, 627, doi:10.1038/s41467-019-08543-0 (2019).
458 9 Patel, P. *et al.* Reproductive phasiRNA loci and DICER-LIKE5, but not microRNA loci,
459 diversified in monocotyledonous plants. *Plant Physiol* **185**, 1764-1782,
460 doi:10.1093/plphys/kiab001 (2021).
461 10 Pokhrel, S. *et al.* Conserved and non-conserved triggers of 24-nt reproductive phasiRNAs
462 in eudicots. *bioRxiv*, doi.org/10.1101/2021.01.20.427321 (2021).
463 11 Yang, X. *et al.* Widespread occurrence of microRNA-mediated target cleavage on
464 membrane-bound polysomes. *Genome Biol* **22**, 15, doi:10.1186/s13059-020-02242-6
465 (2021).

466 12 Song, X. *et al.* Rice RNA-dependent RNA polymerase 6 acts in small RNA biogenesis
467 and spikelet development. *Plant J* **71**, 378-389, doi:10.1111/j.1365-313X.2012.05001.x
468 (2012).
469 13 Zhang, M. *et al.* CHH DNA methylation increases at 24-*PHAS* loci depend on 24-nt
470 phased small interfering RNAs in maize meiotic anthers. *New Phytol* **229**, 2984-2997,
471 doi:10.1111/nph.17060 (2021).
472 14 Komiya, R. *et al.* Rice germline-specific Argonaute MEL1 protein binds to phasiRNAs
473 generated from more than 700 lincRNAs. *Plant J* **78**, 385-397, doi:10.1111/tpj.12483
474 (2014).
475 15 Fan, Y. *et al. PMS1T*, producing phased small-interfering RNAs, regulates photoperiod-
476 sensitive male sterility in rice. *Proc Natl Acad Sci U S A* **113**, 15144-15149,
477 doi:10.1073/pnas.1619159114 (2016).
478 16 Yadava, P. *et al.* Transgenerational conditioned male fertility of HD-ZIP IV transcription
479 factor mutant *ocl4*: impact on 21-nt phasiRNA accumulation in pre-meiotic maize
480 anthers. *Plant Reprod* **34**, 117-129, doi:10.1007/s00497-021-00406-3 (2021).
481 17 Nan, G. L. *et al.* MS23, a master basic helix-loop-helix factor, regulates the specification
482 and development of the tapetum in maize. *Development* **144**, 163-172,
483 doi:10.1242/dev.140673 (2017).
484 18 Dukowic-Schulze, S. *et al.* Novel meiotic miRNAs and indications for a role of
485 phasiRNAs in meiosis. *Front Plant Sci* **7**, 762, doi:10.3389/fpls.2016.00762 (2016).
486 19 Chitwood, D. H. & Timmermans, M. C. Small RNAs are on the move. *Nature* **467**, 415-
487 419, doi:10.1038/nature09351 (2010).
488 20 Dunoyer, P. *et al.* Small RNA duplexes function as mobile silencing signals between
489 plant cells. *Science* **328**, 912-916, doi:10.1126/science.1185880 (2010).
490 21 Molnar, A. *et al.* Small silencing RNAs in plants are mobile and direct epigenetic
491 modification in recipient cells. *Science* **328**, 872-875, doi:10.1126/science.1187959
492 (2010).
493 22 Dunoyer, P. *et al.* Plant mobile small RNAs. *Cold Spring Harb Perspect Biol* **5**,
494 doi:10.1101/cshperspect.a017897 (2013).
495 23 Kelliher, T. & Walbot, V. Emergence and patterning of the five cell types of the *Zea*
496 *mays* anther locule. *Dev Biol* **350**, 32-49, doi:10.1016/j.ydbio.2010.11.005 (2011).

497 24 Nelms, B. & Walbot, V. Gametophyte genome activation occurs at pollen mitosis I in
498 maize. *bioRxiv*, doi.org/10.1101/2021.07.26.453871 (2021).
499 25 Nelms, B. & Walbot, V. Defining the developmental program leading to meiosis in
500 maize. *Science* **364**, 52-56, doi:10.1126/science.aav6428 (2019).
501 26 Czech, B. & Hannon, G. J. Small RNA sorting: matchmaking for Argonautes. *Nat Rev*
502 *Genet* **12**, 19-31, doi:10.1038/nrg2916 (2011).
503 27 Ma, Z. & Zhang, X. Actions of plant Argonautes: predictable or unpredictable? *Curr*
504 *Opin Plant Biol* **45**, 59-67, doi:10.1016/j.pbi.2018.05.007 (2018).
505 28 Araki, S. *et al.* miR2118-dependent U-rich phasiRNA production in rice anther wall
506 development. *Nat Commun* **11**, 3115, doi:10.1038/s41467-020-16637-3 (2020).
507 29 Sun, W. *et al.* Genome-wide identification of AGO18b-bound miRNAs and phasiRNAs
508 in maize by cRIP-seq. *BMC Genomics* **20**, 656, doi:10.1186/s12864-019-6028-z (2019).
509 30 Li, Y. *et al. Male sterile28* encodes an ARGONAUTE family protein essential for male
510 fertility in maize. *Chromosome Res* **29**, 189-201, doi:10.1007/s10577-021-09653-6
511 (2021).
512 31 Moon, J. *et al.* Regulation of cell divisions and differentiation by MALE STERILITY32
513 is required for anther development in maize. *Plant J* **76**, 592-602, doi:10.1111/tpj.12318
514 (2013).
515 32 Huang, K. *et al.* sRNA-FISH: versatile fluorescent in situ detection of small RNAs in
516 plants. *Plant J* **98**, 359-369, doi:10.1111/tpj.14210 (2019).
517 33 Li, N. *et al.* The rice tapetum degeneration retardation gene is required for tapetum
518 degradation and anther development. *Plant Cell* **18**, 2999-3014,
519 doi:10.1105/tpc.106.044107 (2006).
520 34 Xu, J. *et al.* The *ABORTED MICROSPORES* regulatory network is required for
521 postmeiotic male reproductive development in *Arabidopsis thaliana*. *Plant Cell* **22**, 91-
522 107, doi:10.1105/tpc.109.071803 (2010).
523 35 Niu, N. *et al.* EAT1 promotes tapetal cell death by regulating aspartic proteases during
524 male reproductive development in rice. *Nat Commun* **4**, 1445, doi:10.1038/ncomms2396
525 (2013).
526 36 Mamun, E. A. *et al.* Cellular organisation in meiotic and early post-meiotic rice anthers.
527 *Cell Biol Int* **29**, 903-913, doi:10.1016/j.cellbi.2005.08.001 (2005).

528 37 Sager, R. & Lee, J. Y. Plasmodesmata in integrated cell signalling: insights from
529 development and environmental signals and stresses. *J Exp Bot* **65**, 6337-6358,
530 doi:10.1093/jxb/eru365 (2014).
531 38 Long, J. *et al.* Nurse cell--derived small RNAs define paternal epigenetic inheritance in
532 *Arabidopsis*. *Science* **373**, doi:10.1126/science.abh0556 (2021).
533 39 Kelliher, T. & Walbot, V. Hypoxia triggers meiotic fate acquisition in maize. *Science*
534 **337**, 345-348, doi:10.1126/science.1220080 (2012).
535 40 Schneider, C. A. *et al.* NIH Image to ImageJ: 25 years of image analysis. *Nat Methods* **9**,
536 671-675, doi:10.1038/nmeth.2089 (2012).
537 41 Dawe, R. K. *et al.* Meiotic chromosome pairing in maize is associated with a novel
538 chromatin organization. *Cell* **76**, 901-912, doi:10.1016/0092-8674(94)90364-6 (1994).
539 42 Hashimshony, T. *et al.* CEL-Seq2: sensitive highly-multiplexed single-cell RNA-Seq.
540 *Genome Biol* **17**, 77, doi:10.1186/s13059-016-0938-8 (2016).
541 43 Kivioja, T. *et al.* Counting absolute numbers of molecules using unique molecular
542 identifiers. *Nat Methods* **9**, 72-74, doi:10.1038/nmeth.1778 (2011).
543 44 Chen, S. *et al.* fastp: an ultra-fast all-in-one FASTQ preprocessor. *Bioinformatics* **34**,
544 i884-i890, doi:10.1093/bioinformatics/bty560 (2018).
545 45 Aronesty, E. Comparison of sequencing utility programs. *Open Bioinformatics j.* **7**, 1-8,
546 doi: 10.2174/1875036201307010001(2013).
547 46 Pertea, M. *et al.* Transcript-level expression analysis of RNA-seq experiments with
548 HISAT, StringTie and Ballgown. *Nature Protoc* **11**, 1650-1667,
549 doi:10.1038/nprot.2016.095 (2016).
550 47 Mathioni, S. M. *et al.* Characterization of plant small RNAs by next generation
551 sequencing. *Curr Protoc Plant Biol* **2**, 39-63, doi:10.1002/cppb.20043 (2017).
552 48 Bolger, A. M. *et al.* Trimmomatic: a flexible trimmer for Illumina sequence data.
553 *Bioinformatics* **30**, 2114-2120, doi:10.1093/bioinformatics/btu170 (2014).
554 49 Kersey, P. J. *et al.* Ensembl Genomes 2016: more genomes, more complexity. *Nucleic*
555 *Acids Res* **44**, D574-580, doi:10.1093/nar/gkv1209 (2016).
556 50 Tello-Ruiz, M. K. *et al.* Gramene 2018: unifying comparative genomics and pathway
557 resources for plant research. *Nucleic Acids Res* **46**, D1181-D1189,
558 doi:10.1093/nar/gkx1111 (2018).

559 51 Markey, F. B. *et al.* Fusion FISH imaging: single-molecule detection of gene fusion
560 transcripts *in situ*. *PLoS One* **9**, e93488, doi:10.1371/journal.pone.0093488 (2014).
561 52 Batish, M. *et al.* Single molecule imaging of RNA in situ. *Methods Mol Biol* **714**, 3-13,
562 doi:10.1007/978-1-61779-005-8_1 (2011).

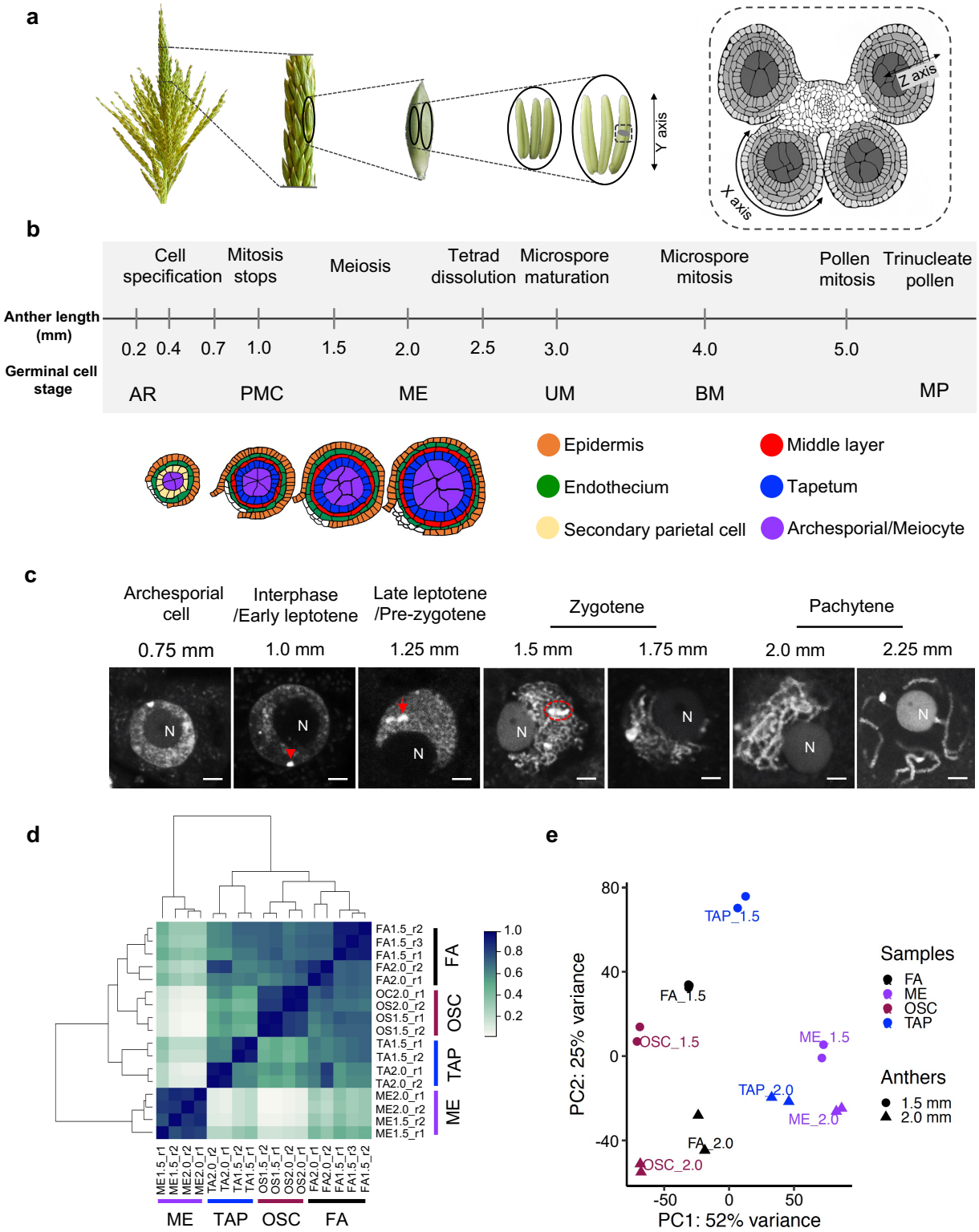

Fig. 1. Staging of maize anthers and quality evaluation of LCM cell sample collections. (a) Male inflorescence structures. From left to right: maize tassel; central spike; single spikelet; three

566 lower and three larger upper florets; transverse confocal microscopy view of a single anther (near
567 the start of meiosis). (**b**) The timeline of maize anther development from initial cell specification,
568 proliferation, and differentiation to pollen maturation. Approximately 10 days of development
569 occur between anther initiation and the start of meiosis at 1.2 mm; meiosis requires 6 days and
570 finishes at 2.5 mm with the tetrad stage; an additional 15-16 days are required for microspore
571 and then pollen development (note that this portion of the timeline is not drawn to scale).
572 Tracings of confocal images of single anther lobes are shown through the dyad stage. The
573 germinal cell stages are abbreviated as follows: mitotic archesporial cells (AR); post-mitotic
574 pollen mother cells (PMC); meiocytes (ME); uninucleate microspore (UM); binucleate
575 microspore (BM); and mature pollen (MP). (**c**) Fluorescence microscopy images of germinal
576 cells visualized with Hoechst staining. During the meiotic proliferation period (0.75 mm anther),
577 archesporial cells have a central nucleolus (N) and a smaller volume than meiotic nuclei. At
578 premeiotic interphase/ early leptotene, the knobs (arrowhead) are round, the nucleoli are located
579 centrally, and chromatin threads are not visible or visible only as localized patches. During
580 leptotene leading to pre-zygotene, the spherical knobs become elongated (arrowhead) coincident
581 with nucleolar movement to the periphery. During zygotene, the knobs are paired (red dashed
582 oval); chromosomes are observed as condensation proceeds. Fully paired bivalents (4 strands per
583 thread) and finally a centrally located nucleolus were observed at pachytene. Scale bar represents
584 2 µm. (**d**) Sample-sample correlation analysis in fixed anthers and LCM cell sample collections
585 at the 1.5 mm and 2.0 mm stages. As shown in the heatmap, the biological replicates of the same
586 sample type are highly correlated at both stages. The scale based on the Pearson correlation is
587 from lightest (no correlation) to darkest (1.0 correlation). Abbreviations: fixed anthers (FA);
588 meiocytes (ME); tapetum (TAP); and other somatic cells (OSC). (**e**) Principal component
589 analysis (PCA) to evaluate the similarity of biological replicates.

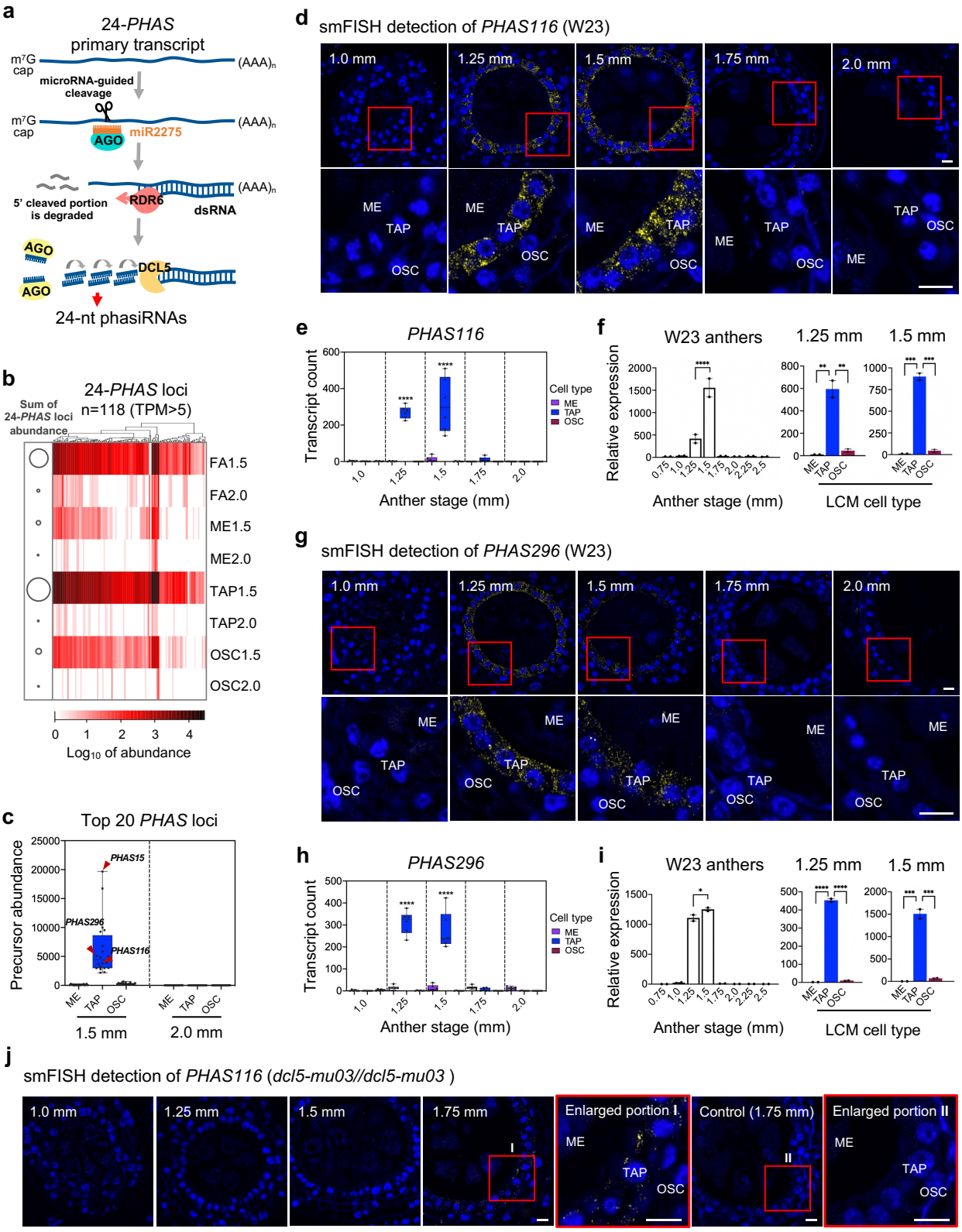

Fig. 2. 24-*PHAS* precursor distribution in maize anthers. (**a**) 24-nt phasiRNA biogenesis

592 pathway. miR2275 is complementary to a conserved motif in precursors, resulting in precise
593 cleavage; cleaved products are converted to double stranded molecules by RNA-dependent RNA
594 polymerase 6 (RDR6). Unknown Argonaute (AGO) proteins participate in biogenesis and bind at
595 least a subset of the 24-nt phasiRNA products. (**b**) Heat map depicting the abundances of 118 24-
596 *PHAS* precursors (TPM > 5 in at least one sample) in fixed anthers and LCM cells. Solid bubbles
597 on the left represent the total abundance of 24-*PHAS* precursors in that sample. (**c**) Boxplot
598 depicts the distribution of the 20 most abundant 24-*PHAS* precursors in LCM cell collections.
599 Arrowheads point to the three 24-*PHAS* loci (*PHAS15*, *PHAS116*, and *PHAS296*) chosen to
600 represent different abundances for RT-qPCR and single-molecule FISH (smFISH) verifications.
601 (**d**) and (**g**) smFISH was performed using probes conjugated with dye Alexa Fluor 647 (AF647)
602 against *PHAS116* and *PHAS296* in W23 maize anthers (1.0-2.0 mm). The fluorescent
603 micrographs were taken using laser scanning confocal microscopy. Below the images are
604 enlargements of area in red rectangles. Yellow smFISH spots correspond to precursor transcripts,
605 which primarily accumulate in TAP. Scale bars = 10 μm. (**e**) and (**h**) Quantification analysis of
606 images in panel **d** and **g**. Transcript counts show the binding events for each cell type at different
607 anther stages using spot count in ImageJ. Two biological and three technical replicates were
608 performed for each stage. Statistical analysis was performed with Prism 8 software. *P* values
609 were determined using one-way ANOVA and Tukey tests. Differences among three cell sample
610 collections within the same anther stage were considered significant for *P* values ≤ 0.05 (* $P \leq$
611 0.05; ** $P \leq 0.01$; *** $P \leq 0.001$; **** $P \leq 0.0001$). (**f**) and (**I**) Quantification of localization of
612 *PHAS116* and *PHAS296* in whole anthers (0.75- 2.5 mm) and LCM cells (1.25 and 1.5 mm) by
613 RT-qPCR. The expression patterns of these 24-*PHAS* precursors are very similar, with high
614 expression levels in tapetum at 1.25 mm, with a peak at the 1.5 mm stage. The tapetal cell
615 sample is significantly higher than either meiocytes or other somatic cells. *P* values were
616 determined using one-way ANOVA and Tukey tests in Prism 8 software. Differences among the
617 samples were considered significant for *P* values ≤ 0.05 (* $P \leq 0.05$; ** $P \leq 0.01$; *** $P \leq 0.001$;
618 **** $P \leq 0.0001$). Note that there is a different scale for each locus. The reference gene
619 (*ZmCyanase*) was used to normalize expression for the accurate assessment of target *24-PHAS*
620 locus expression. (**j**) smFISH detection of *PHAS116* in homozygous *dcl5-mu03//dcl5-mu03*
621 anthers. The red boxes labeled I and II are enlarged in the adjacent image to the right. No signal
622 was detected in control hybridization assays (*Dcl5* probes) at 1.75 mm stage anthers. Scale bars
623 = 10 μm.

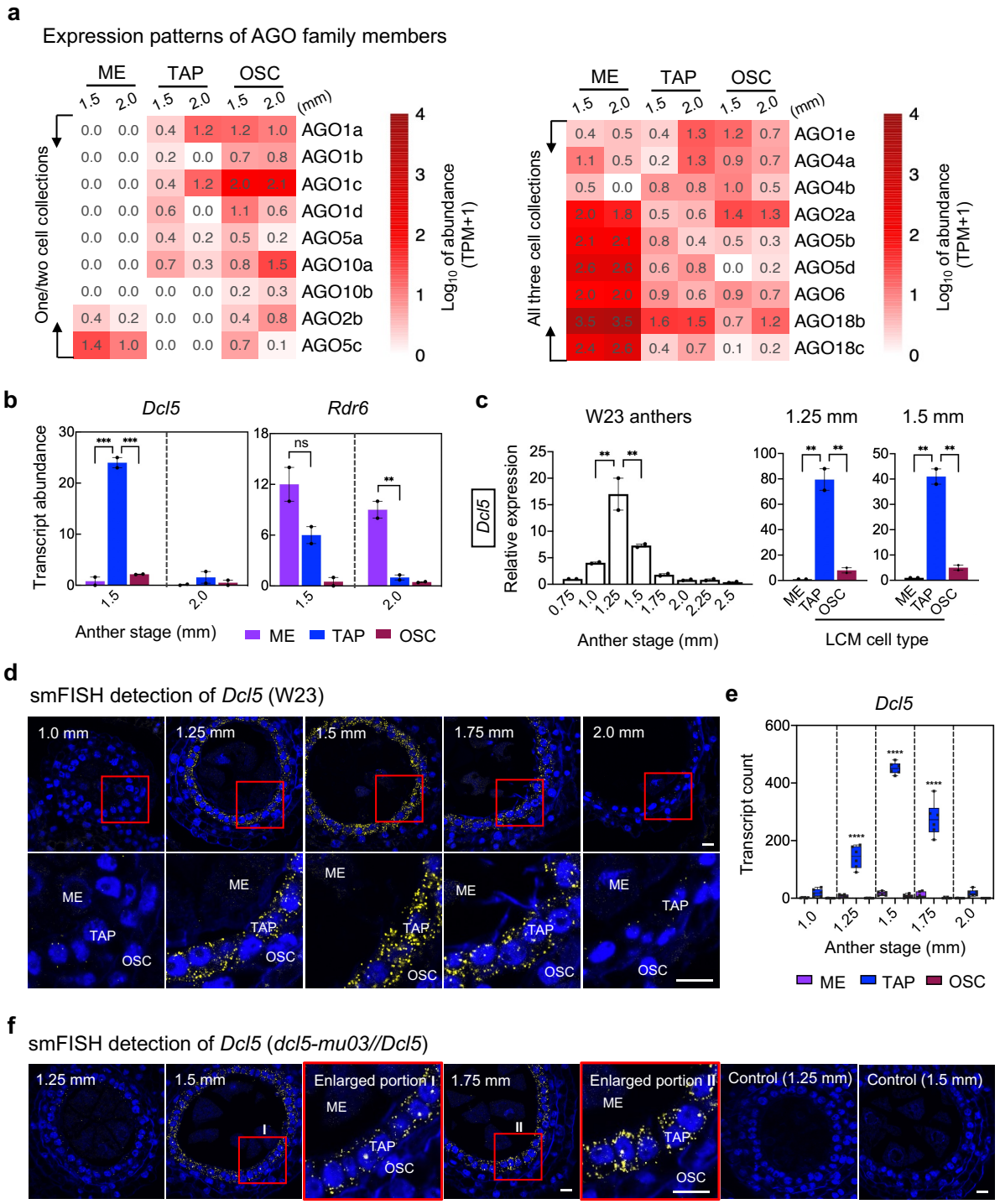

Fig. 3. Evaluation of Argonaute, *Dcl5*, and *Rdr6* expression and *Dcl5* transcript localization in maize anthers. (**a**) RNA abundance from the 18 maize loci encoding Argonaute proteins (AGO). At least one AGO participates in phasiRNA biogenesis by binding miR2275 and a few others have been shown to bind 24-nt phasiRNAs (see text). (**b**) Transcript abundances in LCM cells for two biogenesis genes from RNA-seq datasets. *Dcl5* was highly expressed in 1.5 mm

630 TAP, and *Rdr6* was enriched in both ME and TAP. Differences among the LCM cell samples
631 were considered significant for P values ≤ 0.05 (* $P \leq 0.05$; ** $P \leq 0.01$; *** $P \leq 0.001$; **** P
632 ≤ 0.0001) using one-way ANOVA followed by Tukey tests. (**c**) RT-qPCR analysis for *Dcl5* at
633 multiple anther stages and in LCM cell samples. The tapetal cell samples are significantly higher
634 than ME and OSC (** $P \leq 0.01$). Note that each graph has a different scale. (**d**) and (**e**) smFISH
635 detection and quantification analysis for *Dcl5* transcripts in W23 maize anthers (1.0-2.0 mm).
636 Probes are conjugated with Texas Red dye. The images below each panel are the enlarged
637 portions of red rectangle areas. Yellow smFISH spots correspond to *Dcl5* transcripts are
638 significantly higher in TAP (*** $P \leq 0.001$). Scale bars = 10 µm. (**f**) smFISH detection of *Dcl5*
639 transcripts in homozygous *dcl5-mu03//dcl5-mu03* anthers. Probes are conjugated with Texas Red
640 dye. The red boxes designated as I and II indicate the area enlarged in the adjacent image. To
641 validate the lack of *Dcl5* transcripts, no signal was detected in a control hybridization assay
642 utilizing *Dcl5* probes applied to homozygous *dcl5-mu03//dcl5-mu03* anthers. Scale bars = 10 µm.

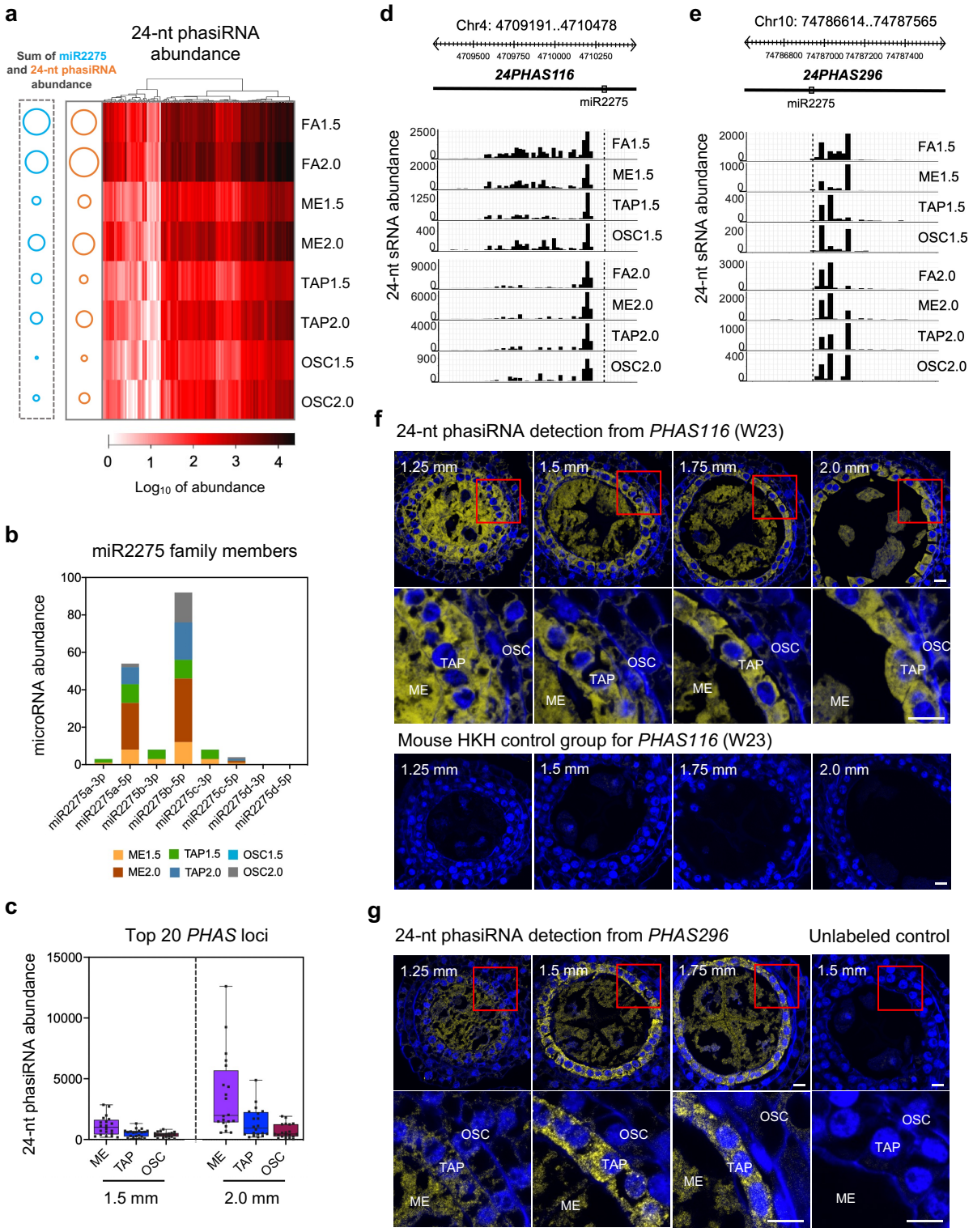

Fig. 4. 24-nt phasiRNA distribution in maize anthers. (**a**) Heat map depicting 24-nt phasiRNA abundance from 118 24-*PHAS* loci in fixed anthers and LCM cell sample collections. Solid bubbles on the left represent the total abundance of miR2275 family members and 24-nt

647 phasiRNAs in that sample. The highest levels of 24-nt phasiRNAs and miR2275 family members
648 are in 2.0 mm meiocytes, followed by tapetum at this stage. (**b**) The abundance of miR2275
649 family members in three LCM cell sample collections. (**c**) Box plot depicting the distribution of
650 24-nt phasiRNAs from the 20 most abundant 24-*PHAS* loci (same as panel **2c**). (**d**) and (**e**) 24-nt
651 sRNA distributions from *PHAS116* and *PHAS296* in FA and LCM cells. The dotted lines
652 represent the miR2275 cleavage sites, and each of the grid lines are spaced 24- nucleotide apart.
653 The accumulation of 24-nt sRNA fragments generated from the same locus are not uniform: only
654 a few of the 24-nt sRNAs show high abundance despite the expectation of equal stoichiometry
655 from a single precursor molecule (15). Overall, accumulation patterns are similar in fixed anthers
656 and LCM cells at each locus. (**f**) 24-nt phasiRNA localization from *PHAS116* in W23 maize
657 anthers (1.25-2.0 mm). Probes are conjugated with Texas Red dye. The red box in each image is
658 enlarged in the panel immediately below each image. Below are negative control images
659 obtained with probes against mouse Hexokinase H (HKH) RNA in W23 maize anthers (1.25-2.0
660 mm). Yellow smFISH spots corresponding to 24-nt phasiRNAs are expressed in all three cell
661 types. Scale bars = 10 µm. (**g**) 24-nt phasiRNA localization from *PHAS296* in W23 maize
662 anthers (1.25-1.75 mm). Probes are conjugated with Texas Red dye. The red box in each image
663 is enlarged in the panel immediately below each image. Yellow smFISH spots corresponding to
664 24-nt phasiRNAs are expressed in all three cell types. No signal was detected in an unlabeled
665 control hybridization. Scale bars = 10 µm.
666

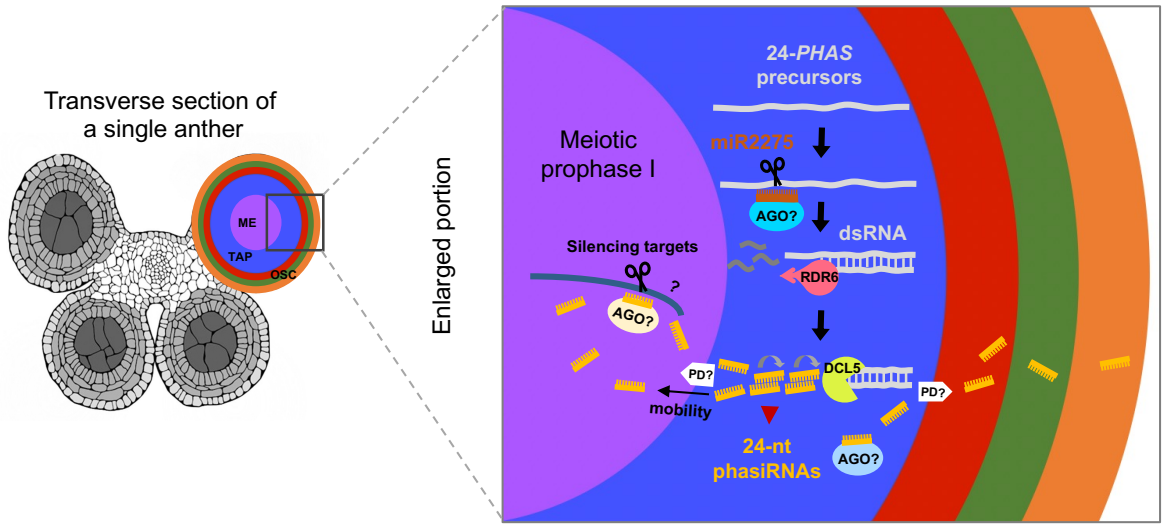

667
668 **Fig. 5. Model of 24-nt phasiRNAs biogenesis and mobility in maize anthers.** On the left is a
669 colorized confocal image as a transverse section of a single anther. On the right is an
670 enlargement of a portion of a single lobe using the same color scheme. During the leptotene-
671 zygotene transition, 24-nt phasiRNAs are generated in TAP and are proposed to move to other
672 cell types. The 30 TAP cells in contact with each meiocyte are proposed to each export a small
673 fraction of their 24-nt phasiRNAs to ME; similarly, a small amount of TAP 24-nt phasiRNA is
674 exported to first to the adjacent Middle Layer (ML) and then distributed to other OSC.

675 **<u>Supplementary information</u>**
676
677 **Supplementary Figures**
678
679 **Supplementary Fig. 1.** Sequential application of LCM to isolate ME, TAP, and OSC in 1.5 mm
680 and 2.0 mm W23 anthers.
681
682 **Supplementary Fig. 2.** Transcript abundances of three *24-PHAS* loci (*PHAS15*, *PHAS116*, and
683 *PHAS296*) in LCM cell sample collections in RNA-seq data.
684
685 **Supplementary Fig. 3.** *PHAS15* localization in maize anthers.
686
687 **Supplementary Fig. 4.** Negative control hybridization assay.
688
689 **Supplementary Fig. 5.** *ZmCyanase* localization in maize anthers.
690
691 **Supplementary Fig. 6.** No labeled control hybridization assay.
692
693 **Supplementary Fig. 7.** *Dcl5* localization in maize anthers.
694
695 **Supplementary Fig. 8.** The distribution of four tapetal-enriched TFs (*Ms23*, *Ms32*, *bHLH51*,
696 and *bHLH122*) in LCM cell sample collections at 1.5 mm and 2.0 mm in RNA-seq data.
697
698 **Supplementary Fig. 9.** sRNA distribution in maize anthers.
699
700 **Supplementary Fig. 10.** 24-nt phasiRNAs localization in maize anthers.
701
702
703 **Supplementary Tables**
704
705 **Supplementary Table 1.** List of LCM cell sample collections from 1.5 mm and 2.0 mm maize
706 anthers.
707
708 **Supplemental Table 2.** Summary of RNA-seq and sRNA-seq libraries prepared from FA and
709 LCM cell sample collections.
710
711 **Supplementary Table 3.** Coordinates and abundance of the 126 24-*PHAS* loci and their
712 corresponding 24-nt phasiRNAs in FA and LCM cells.
713
714 **Supplementary Table 4.** Primer sequences for CEL-seq 2 library preparation.
715
716 **Supplementary Table 5.** Primer sequences for RT-qPCR by the TaqMan assay.
717
718 **Supplementary Table 6.** Probes sequences (5'-> 3') used for smFISH or sRNA-FISH.